



Properties of ZnO/Al₂O₃ Alloy Films Grown Using Atomic Layer Deposition Techniques

J. W. Elam,^a D. Routkevitch^{b,*} and S. M. George^{a,c,z}

^aDepartment of Chemistry and Biochemistry and ^cDepartment of Chemical Engineering, University of Colorado, Boulder, Colorado 80309-0215, USA

^bNanomaterials Research, LLC, Longmont, Colorado 80501, USA

By varying the ratio of the constituents, compound films can exhibit a widely tunable range of physical properties. Atomic layer deposition (ALD) techniques are based on sequential, self-limiting surface reactions and can grow compound films. In this study, ZnO/Al₂O₃ alloy films were prepared using ALD techniques. By adjusting the ALD pulse sequence, the ZnO/Al₂O₃ alloy film composition was varied from 0-100% ZnO. These ZnO/Al₂O₃ alloy films are expected to display varying properties because ZnO and Al₂O₃ have very different physical properties. For example, ZnO is a conductor and Al₂O₃ is an insulator. The physical properties of the ZnO/Al₂O₃ alloys were explored using a variety of techniques. The growth rate, refractive index, composition, surface roughness, crystallinity, resistivity and density of the ZnO/Al₂O₃ alloy films could be continuously tuned over the full range of values defined by the pure oxides. The refractive index varied from $n = 2.00$ for pure ZnO to $n = 1.64$ for pure Al₂O₃. The resistivity could be tuned over 18 orders of magnitude from $10^{-2} \Omega \text{ cm}$ for pure ZnO to $10^{16} \Omega \text{ cm}$ for pure Al₂O₃. Anomalies in surface roughness and density vs. Zn content were observed at a Zn content of $\sim 76\%$. These anomalies were attributed, in part, to the etching of Zn by Al(CH₃)₃ during the ZnO/Al₂O₃ alloy film growth.

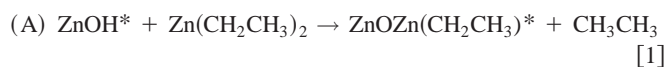
© 2003 The Electrochemical Society. [DOI: 10.1149/1.1569481] All rights reserved.

Manuscript submitted May 31, 2002; revised manuscript received December 16, 2002. Available electronically April 11, 2003.

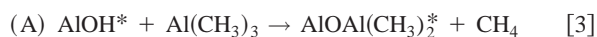
The physical properties of compound films can be tuned by adjusting the relative proportions of the constituent materials. This strategy has been employed to control numerous thin film properties such as refractive index,¹ dielectric constant,² lattice constant,³ hardness,⁴ charge storage capacity,⁵ and surface roughness.⁶ The ability to engineer films with specific physical characteristics impacts a broad range of technologies. These technologies include integrated circuits,^{5,7} optoelectronics,^{3,8} gas sensors,^{9,10} and thermal barrier coatings.^{11,12}

Atomic layer deposition (ALD) is a useful technique for growing compound films. ALD relies on a binary sequence of self-limiting surface chemical reactions.^{13,14} These reactions typically occur between a gas-phase precursor and a solid surface. Films can be deposited by repeating the binary reaction sequence in an ABAB... fashion.^{13,14} Over the last 10-15 years, ALD methods have been developed to deposit numerous materials.¹⁵ The resulting films are usually dense, pinhole-free, and extremely conformal to the underlying substrate. ALD methods also have been used previously to deposit compound films including nanolaminates^{1,5,16-23} alloys,^{2,3,7,8,24-34} complex oxides,³⁵⁻³⁷ and doped materials.³⁸⁻⁴³

ZnO/Al₂O₃ alloys are ideal for exploring the structure-property relationships of ALD compound films. Well-established ALD methods exist for depositing both ZnO⁴⁴⁻⁴⁷ and Al₂O₃⁴⁸⁻⁵² films. ZnO ALD is performed using alternating Zn(CH₂CH₃)₂ and H₂O exposures⁴⁴⁻⁴⁷



where the asterisks represent the surface species. By repeating these reactions in an ABAB... sequence, ZnO films can be deposited with atomic layer control. Al₂O₃ ALD is performed using alternating Al(CH₃)₃ and H₂O exposures⁴⁸⁻⁵²



Al₂O₃ films can be deposited with atomic layer control by repeating these reactions in an ABAB... sequence.

ZnO and Al₂O₃ exhibit very dissimilar physical properties as given in Table I. ZnO ALD films are conducting, crystalline, and rough.⁴⁴⁻⁴⁷ Al₂O₃ ALD films are insulating, amorphous, and smooth.⁴⁸⁻⁵² Because of these differences, the physical properties of ZnO/Al₂O₃ alloys may span a broad range of values. Fortunately, optimal growth rates for ZnO ALD and Al₂O₃ ALD are achieved at nearly the same deposition temperatures and reactant exposures. These similar reaction conditions facilitate the growth of the ZnO/Al₂O₃ alloy films.

ZnO/Al₂O₃ alloy films may have numerous applications. Aluminum-doped ZnO (Al:ZnO) may provide a low cost alternative to indium tin oxide (ITO) as a transparent conducting material for flat panel displays⁵³ and solar cells.⁵⁴ The ZnAl₂O₄ spinel is a widely used catalyst⁵⁵⁻⁵⁷ and catalytic support⁵⁸ material and ZnO is an important semiconducting material for gas sensors.^{59,60} Novel catalysts or gas sensors may result from depositing ZnAl₂O₄ or ZnO on nanoporous substrates. ZnO and Al₂O₃ are both high bandgap materials and are transmissive to visible light. Therefore, ZnO/Al₂O₃ alloy films may benefit optoelectronic applications by allowing the control of refractive index and surface roughness. ZnO/Al₂O₃ alloy films with tunable resistivity may also improve the reliability of microelectromechanical (MEMS) devices by preventing static charge buildup.

This investigation explored the physical properties of the ZnO/Al₂O₃ alloy films. A set of ZnO/Al₂O₃ alloy films was prepared where the percentage of ZnO cycles used to prepare the ZnO/Al₂O₃ alloys was varied from 0-100%. Ellipsometry, stylus profilometry, atomic emission spectroscopy, atomic force microscopy, X-ray diffraction, four-point probe, mercury probe, and *in situ* quartz crystal microbalance measurements were performed to evaluate the film properties. These measurements enabled the determination of the refractive index, surface roughness, crystallinity, resistivity, and density of the ZnO/Al₂O₃ alloy films vs. film composition. The influence of the percentage of ZnO cycles on the thickness and composition of ZnO/Al₂O₃ alloy films was examined in a previous study.⁶¹

Experimental

Viscous flow reactor for atomic layer deposition.—The ZnO/Al₂O₃ alloy films were prepared in a viscous flow ALD reactor

* Electrochemical Society Active Member.

^z E-mail: Steven.George@Colorado.edu

Table I. Physical properties of ZnO and Al₂O₃ ALD films prepared in a viscous flow ALD reactor at 177°C. Surface roughness (rms) is for films deposited using 600 ALD cycles.

Physical property	ZnO	Al ₂ O ₃
Resistivity (Ω cm)	8×10^{-3}	$\sim 10^{16}$
Refractive index	2.00	1.64
Density (g/cm ³)	5.62	2.91
Crystalline phase	Hexagonal	Amorphous
RMS surface roughness (nm)	2.16	0.25
ALD growth rate (Å/cycle)	2.01	1.29

assembled using stainless steel components and conflat seals.⁶² The sample substrates were placed in the flow tube with a 1.4 in. inside diameter that was resistively heated to 177°C. A flow of ~ 200 sccm of filtered, ultrahigh purity nitrogen at a velocity of ~ 2.5 m/s and a pressure of ~ 1 Torr transported the gaseous reactants to the substrates and swept the reaction products into a mechanical pump. The flow reactor was equipped with three independent reactant channels employing computer-controlled solenoid valves to inject the diethyl zinc (DEZ), trimethyl aluminum (TMA), and H₂O precursors into the nitrogen carrier gas. These studies employed Akzo Nobel semiconductor grade DEZ and TMA and Fisher Optima purity H₂O.

ZnO ALD and Al₂O₃ ALD were performed using alternating DEZ/H₂O and TMA/H₂O exposures, respectively, as given by Eq. 1-4. Figure 1 illustrates the reactant pulse sequence employed to deposit a ZnO/Al₂O₃ alloy film with a ZnO cycle percentage of 67%. The DEZ and H₂O pulses alternate and every third DEZ pulse is substituted with a TMA pulse. Consequently, 67% of the metal alkyl pulses are diethyl zinc pulses. Throughout these experiments, the shortest possible pulse sequence was used to obtain the desired ZnO cycle percentage. By interposing the TMA pulses as often as possible while maintaining the desired ZnO cycle percentage, the resulting ZnO/Al₂O₃ alloy should be nearly homogenous.

The ALD ZnO/Al₂O₃ alloy films were deposited on glass and n-doped Si(100) substrates. Reactant exposure times were 1 s and purge times varied between 2-5 s after reactant exposures. Prior to deposition, the glass and Si substrates were degreased using a 15 min dip in a piranha solution containing 70 mL H₂SO₄ and 30 mL of 30% H₂O₂ in H₂O. Subsequently, the Si(100) substrates were etched in a clean room grade, 5% HF/H₂O solution for 1 min to remove the native SiO₂ layer.

The ALD viscous flow reactor was equipped with a quartz crystal microbalance (QCM) allowing *in situ* film growth measurements. Polished QCM sensors from Colorado Crystal Corporation (part no. CCAT1BK-1007-000) were mounted in a Maxtek BSH-150 bakeable sensor head attached to a 2.75 in. conflat flange. The sensor head was modified to provide a nitrogen flow of ~ 20 sccm over the

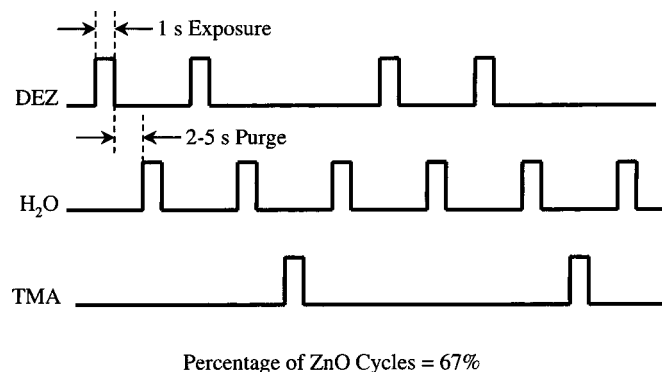


Figure 1. Diagram of ALD pulse sequence for depositing ZnO/Al₂O₃ alloy film where the percentage of ZnO cycles is 67%.

back surface of the sensor crystal. This nitrogen flow prevented deposition on the back side of the sensor. A Maxtek TM400 film thickness monitor interfaced to a computer measured the QCM sensor signals. The thickness monitor and interface allowed mass measurements with a 0.375 ng/cm² resolution at 10 Hz. Assuming a ZnO density of 5.6 g/cm³, this mass resolution equates to a thickness resolution for ZnO of 0.007 Å.

Ex situ measurements.—Elemental analysis was performed on the ZnO/Al₂O₃ alloy films deposited on Si(100) by dissolving some of each film in a 5% hydrofluoric acid/water mixture. The resulting solutions were analyzed by inductively coupled plasma (ICP)-atomic emission spectroscopy (AES). The AES investigations determined the Zn and Al concentrations in each film. These AES measurements allowed the molar Zn content to be evaluated using

$$\text{Zinc film content (\%)} = [\text{Zn}/(\text{Zn} + \text{Al})] \cdot 100\% \quad [5]$$

where Zn and Al are the atomic concentrations of these elements.

Thickness measurements were performed using a Dektak 3 stylus profilometer. Steps were created in the ZnO/Al₂O₃ alloy films using one of two methods. For the films containing higher Zn percentages, a line of Shipley AZ5214E photoresist was applied on top of the alloy film and cured at 100°C for 60 s. Subsequently, the unprotected film was etched away in 10% nitric acid. The photoresist was then removed by sonicating the sample in acetone. The ZnO/Al₂O₃ alloy films containing $\geq 25\%$ Al were insoluble in 10% nitric acid. Although these films could be dissolved in hydrofluoric acid, the hydrofluoric acid also dissolved the photoresist. Consequently, a spot of Shipley AZ5214E photoresist was placed on the Si(100) substrates prior to film growth. After the deposition of these alloy films, the photoresist was removed by rubbing the sample with an acetone-soaked cotton swab.

Sheet resistances for the ZnO/Al₂O₃ alloy films deposited on the glass substrates were measured with a four-point probe. To compute the resistivity from the sheet resistances, the film thicknesses were determined using the stylus profiler. The alloy films containing $\geq 30\%$ Al were too resistive to allow the four-point probe measurements. Consequently, current-voltage measurements were performed on these films deposited on n-doped Si(100) substrates using a mercury microprobe and a picoammeter.⁶³

The surface topography of the alloy films was measured using a Thermomicroscopes Autoprobe CP atomic force microscope in intermittent contact mode. 1×1 μm images were recorded and the root mean squared (rms) roughness was evaluated for each image as described previously.⁶ The thicknesses and refractive indexes for the alloy films deposited on Si(100) substrates were measured using a Rudolph Research Auto EL ellipsometer at a wavelength of 632.8 nm. The crystallinity of the alloy films was evaluated with X-ray diffraction (XRD).

Results

Thickness, composition, and phase.—A set of ZnO/Al₂O₃ alloy films was deposited on Si(100) substrates using a total of 600 ALD cycles. The ZnO cycle percentage was varied from 0–100%. Figure 2 shows the thicknesses measured for the alloy films using ellipsometry (solid circles) and stylus profilometry (open triangles). The ZnO/Al₂O₃ alloy film thickness is relatively constant at ~ 740 – 800 Å for ZnO cycle percentages below $\sim 80\%$. Subsequently, the film thickness increases sharply to ~ 1120 – 1270 Å for films using a ZnO cycle percentage of $\geq 95\%$.

The average growth rates for pure ZnO and pure Al₂O₃ ALD in the viscous flow ALD reactor are 2.01 and 1.29 Å/cycle, respectively.⁶¹ Consequently, the ZnO/Al₂O₃ alloy film thicknesses can be predicted using the rule of mixtures formula:

$$\text{Thickness} = 600 \text{ cycles} \cdot [(2.01 \text{ Å/Cycle})\% \text{ ZnO} + (1.29 \text{ Å/cycle})(100 - \% \text{ ZnO})]/100 \quad [6]$$

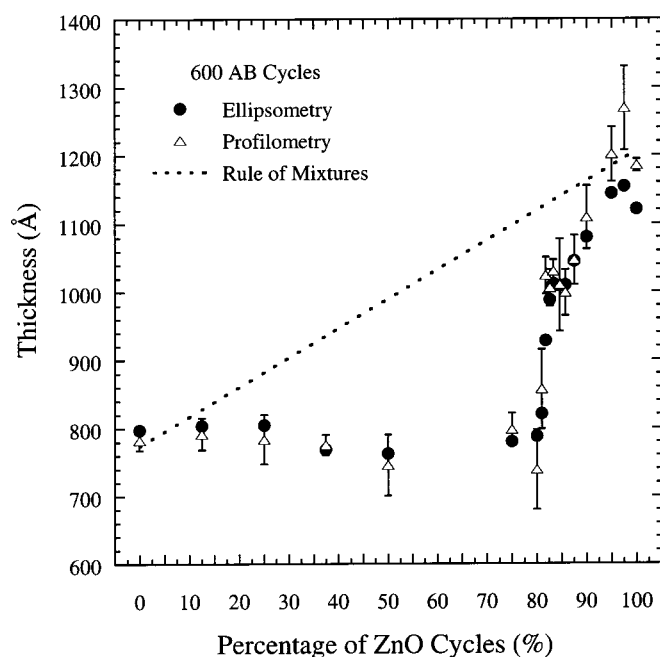


Figure 2. Thickness after 600 AB cycles vs. percentage of ZnO cycles used to grow the ZnO/Al₂O₃ alloy film. The thickness was measured using ellipsometry (solid circles) and stylus profiling (open triangles).

where % ZnO is the percentage of ZnO cycles. The dashed line in Fig. 2 shows the thicknesses predicted by Eq. 6. The measured thicknesses are substantially below the predicted values over most of the range of ZnO cycle percentages.

Portions of the ZnO/Al₂O₃ alloy films prepared on Si(100) substrates using 600 AB cycles at 177°C were dissolved in hydrofluoric acid. The Zn and Al concentrations in the solutions were determined using ICP-AES. The Zn content for each film was calculated from

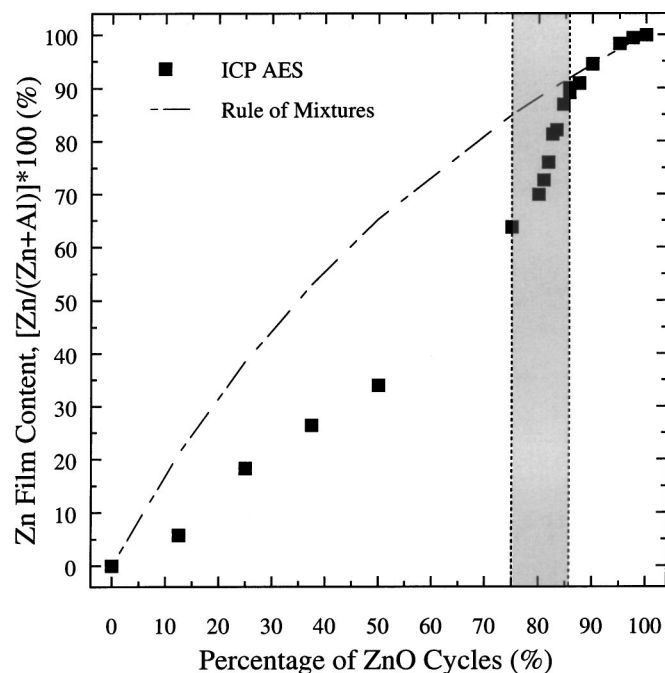


Figure 3. Zn content vs. percentage of ZnO cycles used to grow the ZnO/Al₂O₃ alloy film. The Zn content was determined using ICP-AES.

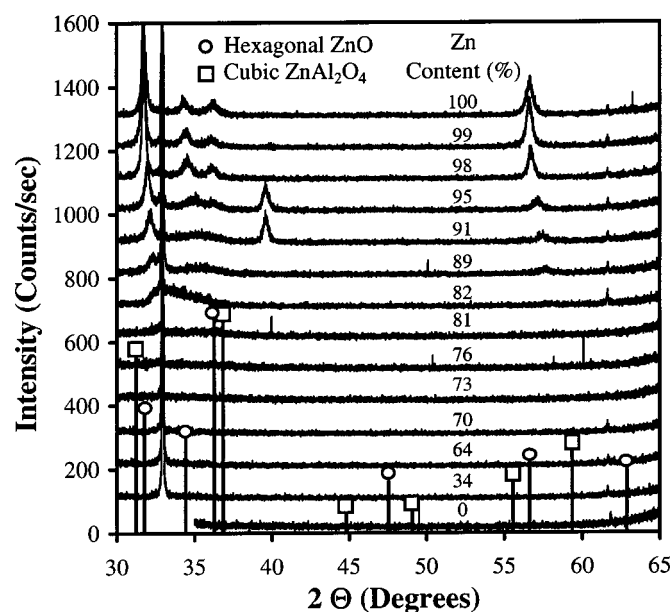


Figure 4. X-ray diffractograms for ZnO/Al₂O₃ alloy films vs. Zn content.

the AES measurements using Eq. 5. The results are given by the solid squares in Fig. 3.

The expected Zn content can be calculated using the rule of mixtures formula

$$\text{Zn film content (\%)} = \frac{\rho_{\text{Zn}}\% \text{ZnO}}{\rho_{\text{Zn}}\% \text{ZnO} + \rho_{\text{Al}}(100 - \% \text{ZnO})} \cdot 100 \quad [7]$$

In this equation, $\rho_{\text{Zn}} = 8.34 \times 10^{14}$ atom/cm² and $\rho_{\text{Al}} = 4.44 \times 10^{14}$ atom/cm². These are the Zn and Al atomic densities deposited during each ALD cycle for the pure ZnO and Al₂O₃ compounds, respectively.⁶¹ For ZnO cycle percentages $\leq 85\%$, the measured Zn content falls below the values predicted by Eq. 7. The gray shaded region in Fig. 3 indicates the range of ZnO cycle percentages where etching was observed during QCM measurements.⁶¹ This etching was evident as a mass loss coincident with each TMA exposure during the ZnO/Al₂O₃ alloy film growth.

Figure 4 shows the X-ray diffractograms for the ZnO/Al₂O₃ alloy films deposited using 600 AB cycles at 177°C on Si(100) substrates. The strong peak at $2\theta = 33^\circ$ and the small peak at 62° in the diffractograms arise from the Si(100) substrate. The accepted locations of the hexagonal ZnO and cubic ZnAl₂O₄ diffraction peaks are indicated by the solid lines with open circles and open squares, respectively. The top trace shows the diffractogram for the pure ZnO film.

The peaks at $2\theta = 32^\circ, 34^\circ, 36^\circ,$ and 56° in Fig. 4 are all characteristic of hexagonal ZnO. The height of the ZnO peak at 56° increases slightly when the Zn content decreases from 100 to 99%. As the Zn content decreases from 99 to 89%, the ZnO features reduce in intensity, broaden, and shift to larger angles. Diffraction peaks from the cubic phase of the ZnAl₂O₄ spinel structure are absent from all of the diffractograms. An unidentified diffraction peak appears at 40° for the alloy films containing 95 and 91% Zn.

Electrical and optical properties.—The solid circles in Fig. 5 plot the resistivities of the ZnO/Al₂O₃ alloy films prepared using 600 AB cycles at 177°C. The resistivities were measured using four-point probe techniques vs. the Zn content as determined from the AES analysis. The resistivity of the pure ZnO films is $8.1 \times 10^{-3} \Omega \text{ cm}$. The resistivity decreases for small additions of Al and reaches a minimum value of $2.2 \times 10^{-3} \Omega \text{ cm}$ at 98% Zn. The resistivity then

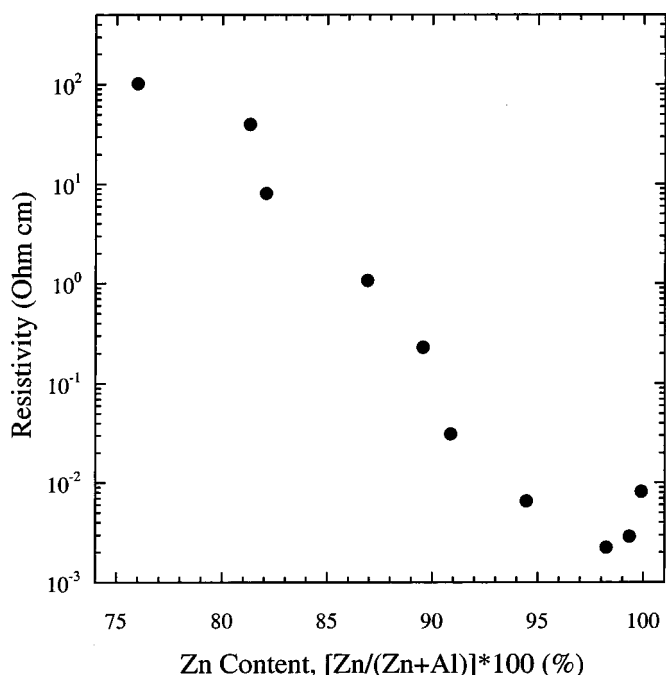


Figure 5. Four-point probe measurements of the resistivity of ZnO/Al₂O₃ alloy films vs. Zn content.

increases for lower Zn content. The ZnO/Al₂O₃ alloy resistivity increases to $1.0 \times 10^2 \Omega \text{ cm}$ for films containing 76% Zn.

The ZnO/Al₂O₃ alloy films with $\leq 75\%$ Zn were not sufficiently conducting to allow four-point probe measurements. Current-voltage measurements were performed on these alloy films using a mercury microprobe and picoammeter. Figure 6 displays current voltage curves for five ZnO/Al₂O₃ alloy films containing 82, 70, 64, 34, and 2.0% Zn deposited on n-doped Si(100) substrates using 600 AB cycles at 177°C. Figure 6 shows that the current density at a given voltage decreases with decreasing Zn percentage.

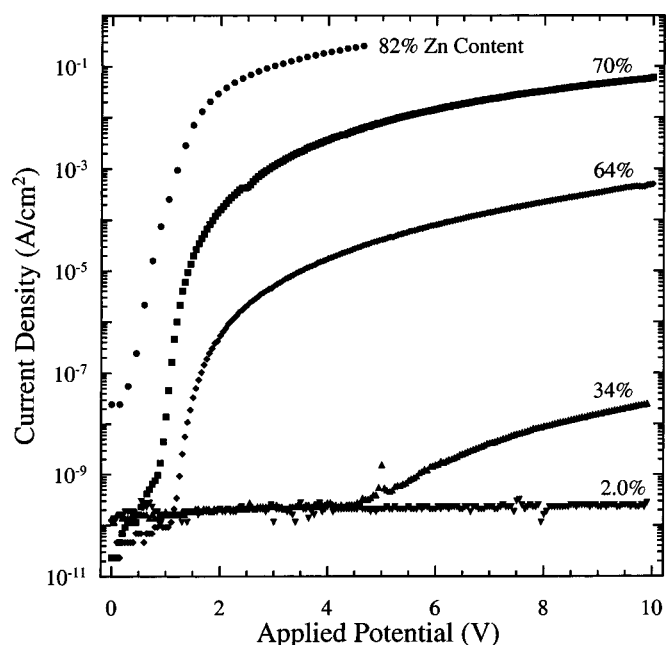


Figure 6. Current-voltage curves measured using the mercury probe for ZnO/Al₂O₃ alloy films with 82, 70, 64, 34, and 2.0% Zn content.

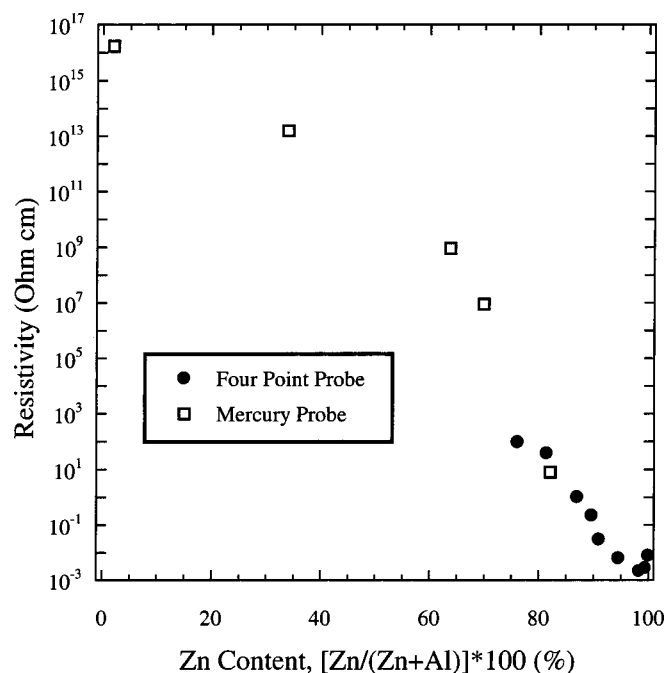


Figure 7. Resistivity of ZnO/Al₂O₃ alloy films measured using the four-point probe and the mercury probe.

The resistivities of the ZnO/Al₂O₃ alloy films can be estimated from the I - V curves in Fig. 6. Most of the I - V curves show a pronounced nonlinearity and the current densities measured at negative voltages are much lower than at positive voltages. In contrast, the I - V curves measured using the mercury probe for films with $\geq 75\%$ Zn content deposited on glass were linear and nearly symmetric with respect to the y axis. These mercury probe measurements also yielded resistivities similar to those obtained using the four-point probe. This similarity indicates a negligible contact resistance at the mercury-alloy film interface. These findings suggest that the asymmetry observed for the films deposited on Si(100) arises from a rectifying junction at the Si-alloy interface. This junction may introduce a contact resistance in series with the alloy film resistance, $R_T = R_C + R_F$ where R_T is the total resistance, R_C is the contact resistance, and R_F is the film resistance.

The slope of the linear portion of the I - V curve for the 82% alloy film at $> 2 \text{ V}$ in Fig. 6 yields $R_T = 2.7 \times 10^3 \Omega$. The resistance of the 82% alloy film can be calculated using $R_F = \rho d/A$ where $\rho = 7.9 \Omega \text{ cm}$ is the resistivity measured using the four-point probe, $d = 1030 \times 10^{-8} \text{ cm}$ is the film thickness, and $A = 4.32 \times 10^{-2} \text{ cm}^2$ is the area of the mercury probe. This equation yields $R_F = 0.019 \Omega$. The contact resistance can then be determined using $R_C = R_T - R_F \sim 2.7 \times 10^3 \Omega$. Assuming that R_C remains constant with Zn content, the resistivities of the alloy films can be calculated from the linear portions of the I - V curves in Fig. 6 after subtracting $R_C \sim 2.7 \times 10^3 \Omega$. The results are displayed in Fig. 7. Figure 7 demonstrates that the resistivity increases nearly exponentially with decreasing Zn content to $1.7 \times 10^{16} \Omega \text{ cm}$ at 2.0% Zn.

Figure 8 presents the refractive index values for the ZnO/Al₂O₃ alloy films deposited on Si(100) using 600 AB cycles at 177°C. These values were obtained using ellipsometry. The refractive index decreases monotonically from $n = 2.00$ at 100% Zn to $n = 1.64$ for the pure Al₂O₃ film. The solid square at 33% Zn marks the location of the refractive index of $n = 1.78$ expected for cubic ZnAl₂O₄ spinel.⁶⁴

Surface roughness and density.—The ZnO/Al₂O₃ alloy films deposited on Si(100) substrates using 600 AB cycles at 177°C were

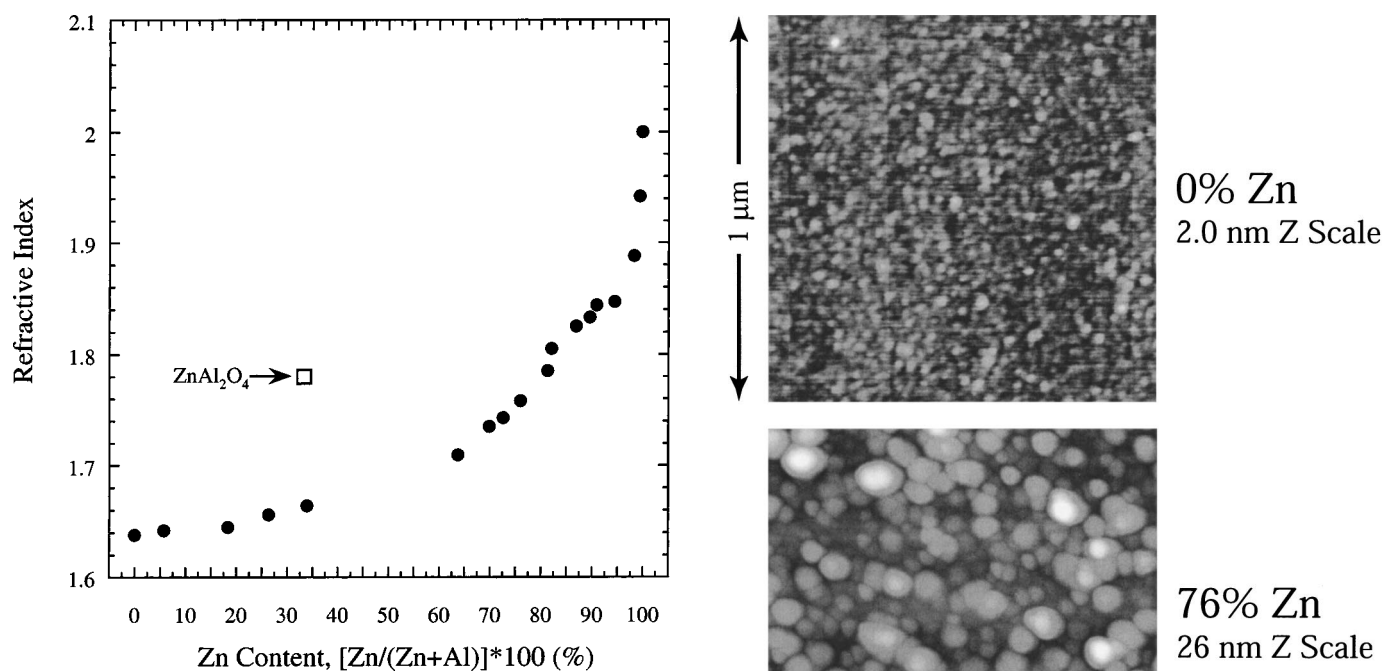


Figure 8. Refractive index of ZnO/Al₂O₃ alloy films vs. Zn content measured using ellipsometry.

analyzed using AFM techniques. Figure 9 shows the topography for $1 \times 1 \mu\text{m}$ AFM images for alloy films with compositions of 0, 76, and 100% Zn. The light-to-dark ranges for these images are 2.0, 26, and 19 nm, respectively. Root mean squared (rms) roughness values calculated from AFM images of ZnO/Al₂O₃ alloy films with Zn contents ranging from 0-100% are shown in Fig. 10. The rms roughness of the pure Al₂O₃ sample is 0.25 nm. In comparison, the rms roughness of the uncoated Si(100) substrate is ~ 0.12 nm. The rms roughness increases with increasing Zn content to 2.2 nm at 100% Zn. In addition, a distinct peak appears at 76% Zn where the surface roughness increases to 3.8 nm.

Densities for the ZnO/Al₂O₃ alloy films were calculated by combining the profilometry thickness measurements with the quartz crystal microbalance (QCM) measurements. The thickness deposited per AB cycle was obtained using the profilometer thickness measurements in Fig. 2. The mass deposited per ALD cycle was obtained using the *in situ* QCM to measure the mass increase for each of the ZnO/Al₂O₃ alloys during ~ 100 ALD cycles. Figure 11 plots the mass deposition rate obtained from the *in situ* QCM measurements as a function of the Zn content determined from the AES analysis. The mass deposition rate of the pure Al₂O₃ film was 37.6 ng/cm²/cycle. The mass deposition rate increases with increasing Zn content and was 113 ng/cm²/cycle for the 100% Zn film.

The solid circles and solid line in Fig. 12 show the ZnO/Al₂O₃ alloy film densities obtained by dividing the mass deposited per ALD cycle by the thickness deposited per ALD cycle. The density of the 100% ZnO film is 5.62 g/cm³. The density decreases with decreasing Zn content to 2.91 g/cm³ for the pure Al₂O₃ film. In addition, there is a pronounced reduction in the density between 70 and 82% Zn. The density reduces to 3.16 g/cm³ at 76% Zn. In comparison, the solid square at 33% Zn content marks the location of the 4.58 g/cm³ density expected for cubic ZnAl₂O₄ spinel.⁶⁴

The expected density for the ZnO/Al₂O₃ alloy films can be calculated using the rule of mixtures formula

$$\text{Density} = \frac{m_{\text{ZnO}}\% \text{ ZnO} + m_{\text{Al}_2\text{O}_3}(100 - \% \text{ ZnO})}{G_{\text{ZnO}}\% \text{ ZnO} + G_{\text{Al}_2\text{O}_3}(100 - \% \text{ ZnO})} \quad [8]$$

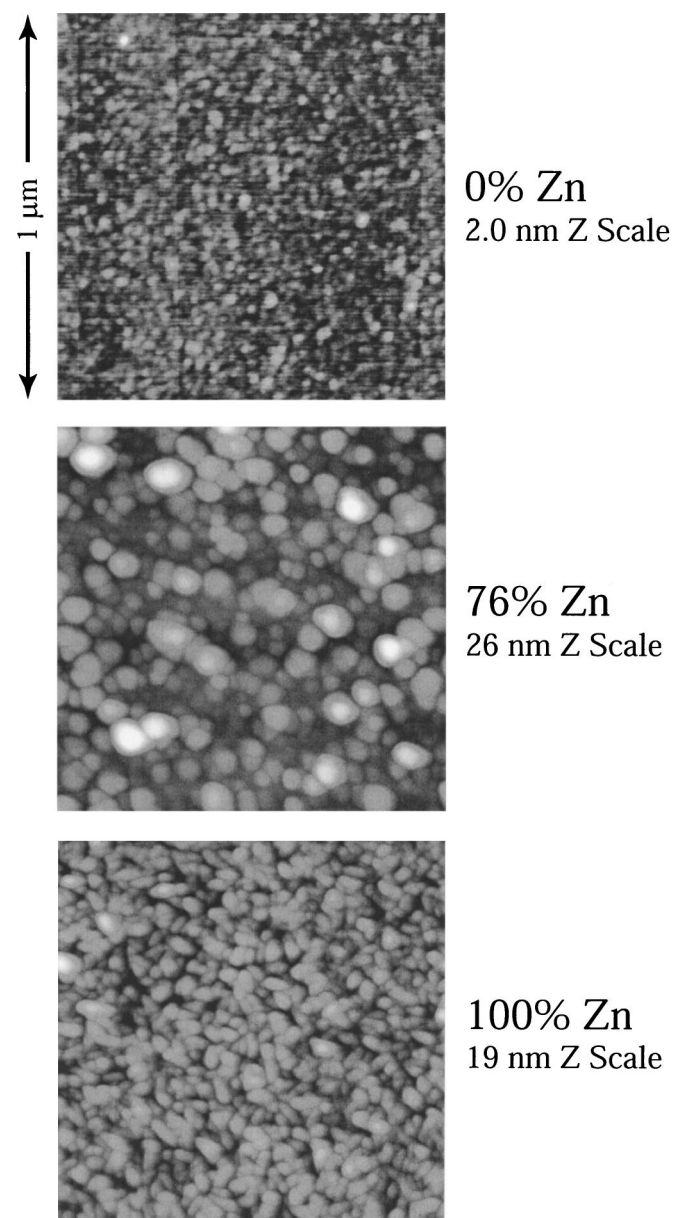


Figure 9. AFM images of ZnO/Al₂O₃ alloy films containing 0 (2.0 nm z scale), 76 (26 nm z scale), and 100% (19 nm z scale) Zn.

In this equation, $m_{\text{ZnO}} = 113 \times 10^{-9}$ g/cm²/cycle and $m_{\text{Al}_2\text{O}_3} = 37.6 \times 10^{-9}$ g/cm²/cycle are the masses deposited per ALD cycle for pure oxide films obtained from QCM measurements.⁶¹ $G_{\text{ZnO}} = 2.01 \times 10^{-8}$ cm/cycle and $G_{\text{Al}_2\text{O}_3} = 1.29 \times 10^{-8}$ cm/cycle are the thicknesses deposited per ALD cycle for the pure oxides.⁶¹ The dotted line in Fig. 12 shows the rule of mixtures density predicted for the ZnO/Al₂O₃ alloy films using Eq. 8. The Zn content is obtained from % ZnO using the relationship between Zn content and % ZnO shown in Fig. 3. The measured densities are significantly lower than the densities predicted by Eq. 8 over most of the range of Zn content.

The alloy film densities can also be predicted from the measured refractive indexes in Fig. 8 using Lorentz-Lorenz analysis.^{65,66} The Lorentz-Lorenz analysis evaluates the refractive index of a compound film from the individual molar refractivities, A , of the components. The molar refractivity of a single component is given by

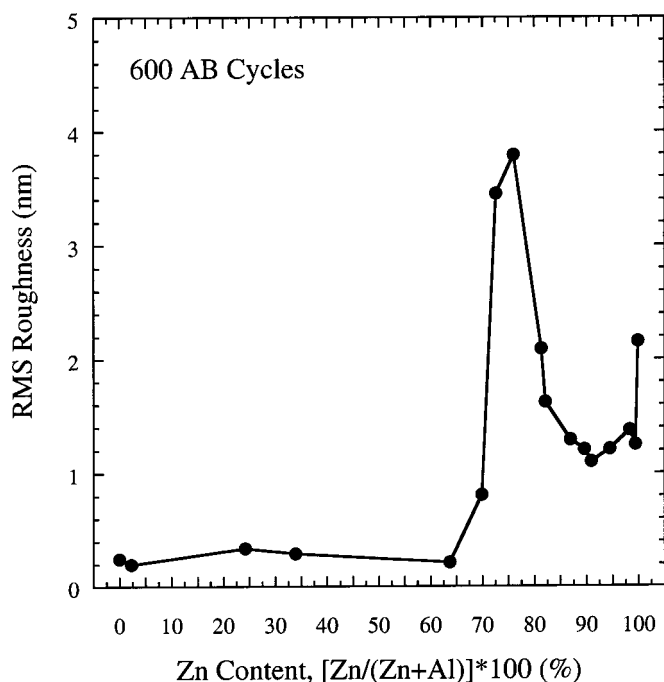


Figure 10. RMS surface roughness of ZnO/Al₂O₃ alloy films vs. Zn content determined by AFM measurements.

$$A = \frac{w(n^2 - 1)}{\rho(n^2 + 2)} \quad [9]$$

where w is molecular weight, ρ is density, and n is refractive index. The molar refractivity of a ZnO/Al₂O₃ alloy film is given by

$$A_{\text{Film}} = X_{\text{ZnO}}A_{\text{ZnO}} + (1 - X_{\text{ZnO}})A_{\text{Al}_2\text{O}_3} = \frac{w_{\text{Film}}(n^2 - 1)}{\rho_{\text{Film}}(n^2 + 2)} \quad [10]$$

In this expression, X_{ZnO} is the mole fraction of ZnO in the film and w_{Film} and ρ_{Film} are the average molecular weight and density of the film, respectively.

The mole fraction of ZnO in the alloy film can be obtained from $X_{\text{ZnO}} = \text{Zn}/(\text{Zn} + 2\text{Al})$ using the Zn and Al concentrations in the alloy films determined by the AES analysis. A_{ZnO} and $A_{\text{Al}_2\text{O}_3}$ were determined from Eq. 9 using the refractive index and density measured for pure ZnO and Al₂O₃ films, respectively. The molar refractivities were $A_{\text{ZnO}} = 7.24$ and $A_{\text{Al}_2\text{O}_3} = 12.62$. The molecular weight for the film, w_{Film} was calculated using X_{ZnO} and the molecular weights of ZnO and Al₂O₃.

Equation 10 can be rearranged to predict the density of the alloy film as a function of the measured refractive indexes. The densities predicted for the ZnO/Al₂O₃ alloy films using the Lorentz-Lorenz analysis are given by the dashed line in Fig. 12. The Lorentz-Lorenz formula predicts the alloy densities reasonably well between 0–65% Zn. However, Eq. 10 fails to account for the distinct reduction in density at 76% Zn. Equation 10 also underestimates the densities of the alloy films between 85–98% Zn.

Discussion

Thickness, composition, and phase.—Figure 2 shows that the thicknesses measured for many of the ZnO/Al₂O₃ alloy films are significantly below the thicknesses predicted by the rule of mixtures formula given by Eq. 6. The alloy films are thinner than the expectations from the growth rates for pure ZnO and Al₂O₃ ALD films.

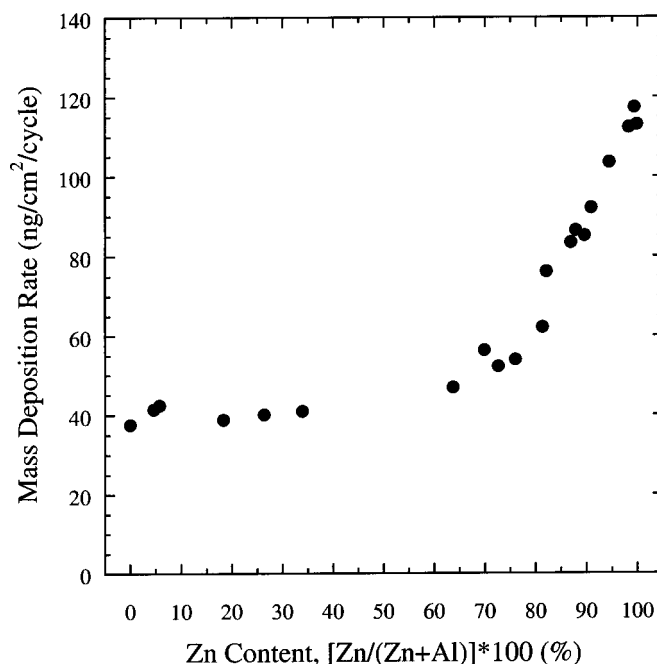


Figure 11. Mass deposition rate of ZnO/Al₂O₃ alloy films vs. Zn content determined by *in situ* QCM measurements.

The smaller thicknesses are explained, in part by the nucleation behavior that occurs when making the transition between ZnO and Al₂O₃.⁶¹ Both ZnO ALD growth on Al₂O₃ and Al-doped ZnO surfaces and Al₂O₃ ALD growth on ZnO and Zn-doped Al₂O₃ surfaces require numerous AB cycles to obtain the bulk ZnO and Al₂O₃ ALD growth rates.

The Zn content shown in Fig. 3 is also below the rule of mixtures prediction given by Eq. 7 for most of the ZnO/Al₂O₃ alloy films. The lower than expected Zn content is attributed to the etching of Zn by TMA.⁶¹ This etching is believed to occur by the reaction

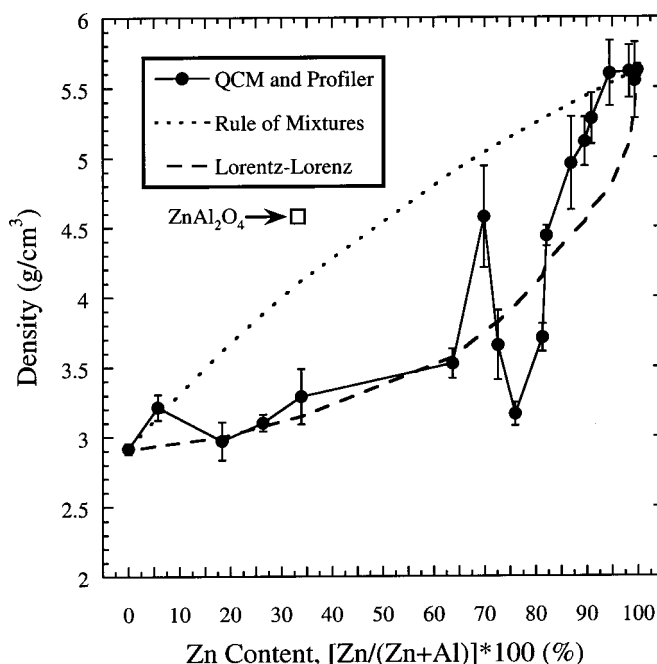


Figure 12. Density vs. Zn content for ZnO/Al₂O₃ alloy films determined by QCM and stylus profiler measurements.



The gray shaded region in Fig. 3 indicates the range of ZnO cycle percentages where etching was observed during QCM measurements. This etching region coincides with the distinct reduction in Zn content in Fig. 3 and alloy film thickness in Fig. 2 compared with the rule of mixtures predictions.

Previous investigations have established that ZnO ALD grows in the hexagonal crystalline phase.^{45,47} In agreement with these previous studies, the diffractogram for the film with 100% ZnO shown in Fig. 4 displays strong peaks at $2\Theta = 32^\circ$ and 56° that are consistent with hexagonal ZnO. The $2\Theta = 56^\circ$ peak height increases slightly when the Al content increases to $\sim 1\%$. This increase may result from a slightly thicker film after 600 AB cycles at 177°C and larger ZnO nanocrystals in the film. In support of this explanation, the profilometry measurements in Fig. 2 show a 7% thickness increase from 1185 to 1269 Å when the ZnO cycle percentage is reduced from 100 to 97.5%.

The ZnO diffraction peaks in Fig. 4 decrease in height and increase in width with increasing Al content. This behavior suggests a loss of crystallinity. The ZnO/Al₂O₃ alloy films appear to be amorphous for Zn contents $\leq 81\%$. These observations are consistent with the previous findings that ZnO ALD is crystalline⁴⁷ and Al₂O₃ ALD is amorphous⁶⁷ under these growth conditions. In the Zn content range of 100–89% where the alloy films display crystallinity, the ZnO diffraction peaks shift to larger angles with increasing Al content. According to Bragg's law, $n\lambda = 2d \sin \Theta$, a decrease in lattice spacing, d , will lead to an increase in the detected peak position, Θ . The Zn²⁺ ionic radius is 0.72 Å and the Al³⁺ ionic radius is 0.53 Å. As predicted by Bragg's law and the smaller ionic radius of Al³⁺, the ZnO XRD peaks shift to larger angles with increasing Al content.

Electrical and optical properties.—Figure 5 shows that the resistivity of the ZnO/Al₂O₃ alloy film decreases when doped with small amounts of Al. This phenomenon has been observed previously.^{44,53,68} The improved conductivity of the ZnO films results from the n-doping of ZnO by Al ions.^{44,53,68} When a Zn²⁺ ion in the ZnO lattice is replaced by an Al³⁺ ion, the Al³⁺ contributes an extra valence electron as a charge carrier. This theory is supported by Hall probe measurements of Al:ZnO ALD films that exhibit an increase in charge carrier density for small Al percentages.^{44,53,68}

The XRD results shown in Fig. 4 also reveal that the Al³⁺ dopants perturb the ZnO lattice. This perturbation creates scattering sites that decrease the electron mobility and ultimately increase the resistivity. In addition, excess Al doping can create nonconducting Al₂O₃ clusters that do not produce electron donors.^{69,70} When the Zn content is $< 98\%$, Fig. 5 and 7 show that the resistivity of the ZnO/Al₂O₃ alloy film increases nearly exponentially with decreasing Zn content. The resistivity of the 2.0% Zn film is $1.7 \times 10^{16} \Omega \text{ cm}$. This value is similar to the resistivity measured for pure Al₂O₃ ALD films.⁶³ The presence of only a few percent of Zn in Al₂O₃ has a negligible effect on the resistivity of the Al₂O₃ films.

The refractive index of the ZnO/Al₂O₃ alloy films decreases monotonically and relatively smoothly from $n = 2.00$ to $n = 1.64$ with decreasing Zn content as shown in Fig. 8. The refractive indexes measured for the pure ZnO and Al₂O₃ ALD films agree well with previous measurements of $n = 1.95$ for ZnO⁶ and $n = 1.65$ ⁴⁸ for Al₂O₃ ALD films. There is a rapid drop in refractive index between 100–95% Zn. This reduction is not accompanied by a simultaneous reduction in density in Fig. 12. However, the crystallinity decreases significantly for the alloy films between 100–95% Zn content as shown in Fig. 4. These findings suggest that the refractive indexes of these Zn-rich films are more affected by crystallinity than density. The refractive index and thickness values determined using the ellipsometer could be determined more accurately by modeling

the ellipsometric data using the known surface roughnesses presented in Fig. 10.

The refractive index measured for the 34% alloy film in Fig. 8 is $n = 1.66$. This value is significantly below the literature value of $n = 1.78$ for the ZnAl₂O₄ spinel. This large difference suggests that the spinel phase does not form under the ALD conditions used to prepare the ZnO/Al₂O₃ alloy films. The X-ray diffractograms in Fig. 4 also provide no evidence for the cubic ZnAl₂O₄ phase. In addition, Fig. 12 shows that the density of the 34% alloy film is well below the value of 4.58 g/cm³ expected for the ZnAl₂O₄ spinel.

Additional measurements could provide a more detailed understanding of the electrical and optical behaviors of the ZnO/Al₂O₃ alloy films. For instance, optical reflectivity measurements could probe the variation in bandgap with Zn content allowing an examination of the transition between semiconducting and insulating behavior. Capacitance measurements performed using the mercury probe could determine the variation in permittivity of the ZnO/Al₂O₃ alloy films vs. the Zn content. The resistivity values in Fig. 7 derived from the mercury probe measurements assume a constant contact resistance at the interface between the Si substrate and the alloy film. This assumption could be verified by performing supplementary resistance measurements on ZnO/Al₂O₃ alloy film test structures employing vapor deposited Ti/Au electrodes. Ti/Au electrodes form an Ohmic contact with a very low contact resistance when vapor deposited onto Al-doped ZnO films.⁷¹

Surface roughness and density.—Previous investigations have shown that ZnO ALD films roughen considerably with increasing thickness as a result of the growth of ZnO nanocrystals.⁶ In contrast, Al₂O₃ ALD films deposit in an amorphous form and remain remarkably smooth with increasing thickness.⁶ The surface roughness of a particular ZnO film thickness can be made progressively smoother by interleaving Al₂O₃ layers in the ZnO film to increase the number of ZnO/Al₂O₃ interfaces.⁶ The progressive smoothing of the film surface is accompanied by a simultaneous reduction in the intensity of the ZnO diffraction peaks observed in grazing incidence XRD measurements.⁷² These results suggest that the ZnO nanocrystal growth is interrupted by the Al₂O₃ layers. This interruption results in smoother, more amorphous films.

In agreement with these previous results, Fig. 10 shows that the ZnO/Al₂O₃ alloy films become smoother with increasing Al content. However, the prominent peak in rms roughness at 76% Zn content is unexpected and may indicate the formation of a new crystalline phase. Contrary to this expectation, the XRD measurements in Fig. 4 indicate that the ZnO/Al₂O₃ alloy films are amorphous at 76% Zn.

An alternative explanation for the peak in rms roughness shown in Fig. 10 can be found in the density measurements of Fig. 12. Expanded views of these two data sets are superimposed in Fig. 13. The open squares and dotted line plot the rms roughness values. The solid circles and solid line display the density measurements. Figure 13 clearly shows that the peak in rms roughness coincides with the reduction in density. Furthermore, these two features are fairly well bracketed within the range of compositions where etching was observed by the *in situ* QCM measurements.⁶¹ This range is indicated by the dashed lines in Fig. 13.

The increased roughness and decreased density may result from the etching process. The etching of the ZnO/Al₂O₃ alloy films by the TMA pulses appears to remove selectively Zn atoms. This selective removal results in a sudden drop in Zn content below the rule of mixtures estimate shown in Fig. 3. The etching may occur by the reaction given in Eq. 11. The removal of Zn atoms will leave voids that roughen the film surface.

A line scan analysis of the AFM image for the 76% Zn alloy film in Fig. 9 reveals peak-to-valley thickness changes that are $> 200 \text{ Å}$ within a lateral spacing of $\sim 100 \text{ nm}$. These topographical changes are too abrupt to be detected accurately by the stylus profilometer probe tip. The profilometer tip will ride over these surface features and yield thicknesses that are too large. These larger thicknesses

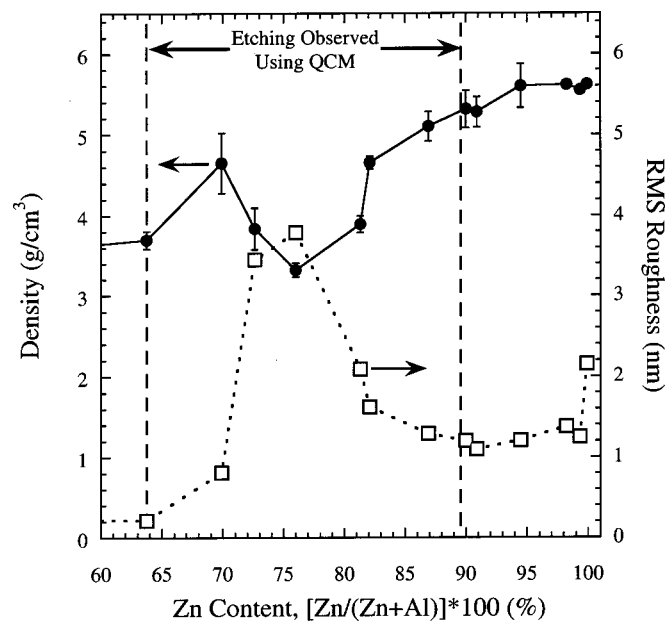


Figure 13. Comparison of density and surface roughness (rms) of ZnO/Al₂O₃ alloy films vs. Zn content between 64-100% Zn.

would yield smaller densities. This explanation partially accounts for the reduction in density at 76% Zn shown in Fig. 13.

The Lorentz-Lorenz density prediction is given by the dashed line in Fig. 12. This prediction is based on the relationship between the density and refractive index as expressed by Eq. 9 and 10.^{65,66} If an artifact in the stylus profilometer measurements caused the measured densities to be low, the measured densities may be below the Lorentz-Lorenz estimates. However, some of the measured densities are larger than the densities obtained from the refractive indexes. In particular, the measured density values are significantly higher than the Lorentz-Lorenz estimates between ~85-99% Zn. These observations argue against the possible stylus profilometer artifact.

A detailed examination of the ZnO/Al₂O₃ alloy film properties was conducted between 70-82% Zn. This investigation revealed that the reduction in density at ~76% Zn results from a combination of an increase in measured thickness and a simultaneous drop in mass deposition rate. This combination suggests that etching may both lower the mass deposition rate and substantially increase the free volume of the ZnO/Al₂O₃ alloy films.

Conclusions

ZnO/Al₂O₃ alloys were grown using ZnO ALD with Zn(CH₂CH₃)₂/H₂O and Al₂O₃ ALD with Al(CH₃)₃/H₂O. The composition of the ZnO/Al₂O₃ alloy films was controlled by adjusting the relative number of ZnO ALD and Al₂O₃ ALD reaction cycles in the pulse sequence. Alloys were grown with physical characteristics that could be tuned over the full range of values defined by pure ZnO and Al₂O₃. A variety of film properties was investigated vs. Zn content including the film growth rate, refractive index, surface roughness, crystallinity, resistivity, and density. The refractive indexes varied from $n = 2.00$ for pure ZnO to $n = 1.64$ for pure Al₂O₃. The resistivities of the ZnO/Al₂O₃ alloy films ranged from $\sim 10^{-3} \Omega \text{ cm}$ for the 98% Zn film to $\sim 10^{16} \Omega \text{ cm}$ for the 2.0% alloy film. This remarkable span of over 18 orders of magnitude for the resistivity may be useful in many thin-film electrical applications. Anomalies in rms surface roughness and density were observed for the alloy films with a Zn content of ~76%. These anomalies may be partially explained by the etching of Zn by Al(CH₃)₃ during the ZnO/Al₂O₃ alloy film growth.

Acknowledgments

This work was funded by the Air Force Office of Scientific Research (AFOSR) and Nanomaterials Research, LLC. Professor John Drexler of the Department of Geological Sciences at the University of Colorado performed the ICP-AES elemental analysis of the alloy films. The authors thank Tom Seidel and Ofer Sneh of Genus, Inc., for donating equipment used to construct the viscous flow ALD reactor.

University of Colorado assisted in meeting the publication costs of this article.

References

- H. Kattelus, M. Ylilammi, J. Saarilahti, J. Antson, and S. Lindfors, *Thin Solid Films*, **225**, 296 (1993).
- M. Stromme, G. A. Niklasson, M. Ritala, M. Leskela, and K. Kukli, *J. Appl. Phys.*, **90**, 4532 (2001).
- H. Fujiwara, T. Nabeta, and I. Shimizu, *Jpn. J. Appl. Phys., Part 1*, **33**, 2474 (1994).
- X. Chu, M. S. Wong, W. D. Sproul, and S. A. Barnett, *J. Mater. Res.*, **14**, 2500 (1999).
- K. Kukli, M. Ritala, and M. Leskela, *J. Appl. Phys.*, **86**, 5656 (1999).
- J. W. Elam, Z. A. Sechrist, and S. M. George, *Thin Solid Films*, **414**, 43 (2002).
- M. Vehkamäki, T. Hatanpää, T. Hanninen, M. Ritala, and M. Leskela, *Electrochem. Solid-State Lett.*, **2**, 504 (1999).
- J. Ihanus, M. Ritala, M. Leskela, and E. Rauhala, *Appl. Surf. Sci.*, **112**, 154 (1997).
- H. Y. Bae and G. M. Choi, *Sens. Actuators B*, **55**, 47 (1999).
- J. H. Yu and G. M. Choi, *Sens. Actuators B*, **75**, 56 (2001).
- S. Sharafat, A. Kobayashi, V. Ogden, and N. M. Ghoniem, *Vacuum*, **59**, 185 (2000).
- F. Wang, L. Wang, and G. Liu, *Surf. Eng.*, **17**, 35 (2001).
- T. Suntola and J. Hyvarinen, *Annu. Rev. Mater. Sci.*, **15**, 177 (1985).
- S. M. George, A. W. Ott, and J. W. Klaus, *J. Phys. Chem.*, **100**, 13121 (1996).
- M. Ritala and M. Leskela, in *Handbook of Thin Film Materials*, H. S. Nalwa, Editor, Academic Press, San Diego, CA (2001).
- M. Ritala, M. Leskela, L. Niinisto, T. Prohaska, G. Friedbacher, and M. Grasserbauer, *Thin Solid Films*, **249**, 155 (1994).
- K. Kukli, J. Ihanus, M. Ritala, and M. Leskela, *Appl. Phys. Lett.*, **68**, 3737 (1996).
- J. M. Hartmann, M. Charleux, H. Mariette, and J. L. Rouviere, *Appl. Surf. Sci.*, **112**, 142 (1997).
- M. Ishii, S. Iwai, H. Kawata, T. Ueki, and Y. Aoyagi, *J. Cryst. Growth*, **180**, 15 (1997).
- H. Kumagai, K. Toyoda, K. Kobayashi, M. Obara, and Y. Imura, *Appl. Phys. Lett.*, **70**, 2338 (1997).
- H. Zhang, R. Solanki, B. Roberds, G. Bai, and I. Banerjee, *J. Appl. Phys.*, **87**, 1921 (2000).
- K. Kukli, M. Ritala, and M. Leskela, *J. Electrochem. Soc.*, **148**, F35 (2001).
- H. Zhang and R. Solanki, *J. Electrochem. Soc.*, **148**, F63 (2001).
- B. T. McDermott, K. G. Reid, N. A. El-Masry, S. M. Bedair, W. M. Duncan, X. Yin, and F. H. Pollak, *Appl. Phys. Lett.*, **56**, 1172 (1990).
- H. Kattelus, M. Ylilammi, J. Salmi, T. Ranta-Aho, E. Nykanen, and I. Suni, *Mater. Res. Soc. Symp. Proc.*, **284**, 511 (1993).
- H. Fujiwara, T. Nabeta, H. Kiryu, and I. Shimizu, *Jpn. J. Appl. Phys., Part 1*, **33**, 4381 (1994).
- T. Asikainen, M. Ritala, and M. Leskela, *J. Electrochem. Soc.*, **142**, 3538 (1995).
- K. S. Boutsos, F. G. McIntosh, J. C. Roberts, S. M. Bedair, E. L. Piner, and N. A. El-Masry, *Appl. Phys. Lett.*, **67**, 1856 (1995).
- H. Seim, M. Nieminen, L. Niinisto, H. Fjellvag, and L.-S. Johansson, *Appl. Surf. Sci.*, **112**, 243 (1997).
- H. Seim, H. Molsa, M. Nieminen, H. Fjellvag, and L. Niinisto, *J. Mater. Chem.*, **7**, 449 (1997).
- O. Nilsen, M. Peussa, H. Fjellvag, L. Niinisto, and A. Kjekshus, *J. Mater. Chem.*, **9**, 1781 (1999).
- J. H. Song, E. D. Sim, K. S. Baek, and S. K. Chang, *J. Cryst. Growth*, **214**, 460 (2000).
- M. Schuisky, K. Kukli, M. Ritala, A. Harsta, and M. Leskela, *Chem. Vap. Deposition*, **6**, 139 (2000).
- M. Juppo, P. Alen, M. Ritala, and M. Leskela, *Chem. Vap. Deposition*, **7**, 211 (2001).
- S. Haukka, M. Lindblad, and T. Suntola, *Appl. Surf. Sci.*, **112**, 23 (1997).
- M. Nieminen, T. Sajavaara, E. Rauhala, M. Putkonen, and L. Niinisto, *J. Mater. Chem.*, **11**, 2340 (2001).
- A. Rahtu, T. Hanninen, and M. Ritala, *J. Phys. IV*, **11**, 923 (2001).
- T. Suntola and A. Jorma, U.S. Pat. 4,058,430 (1977).
- H. Viirola and L. Niinisto, *Thin Solid Films*, **251**, 127 (1994).
- W. Kong, J. Fogarty, and R. Solanki, *Appl. Phys. Lett.*, **65**, 670 (1994).
- K.-E. Elers, M. Ritala, M. Leskela, and E. Rauhala, *Appl. Surf. Sci.*, **82/83**, 468 (1994).
- D. Jung, M. Leonard, N. E. El-Masry, and S. M. Bedair, *J. Electron. Mater.*, **24**, 75 (1995).
- E. B. Yousfi, B. Weinberger, F. Donsanti, P. Cowache, and D. Lincot, *Thin Solid Films*, **387**, 29 (2001).
- V. Lujala, J. Skarp, M. Tammenmaa, and T. Suntola, *Appl. Surf. Sci.*, **82/83**, 34 (1994).

45. A. Yamada, B. Sang, and M. Konagai, *Appl. Surf. Sci.*, **112**, 216 (1997).
46. A. W. Ott and R. P. H. Chang, *Mater. Chem. Phys.*, **58**, 132 (1999).
47. E. B. Yousfi, J. Fouache, and D. Lincot, *Appl. Phys. Lett.*, **153**, 223 (2000).
48. A. W. Ott, J. W. Klaus, J. M. Johnson, and S. M. George, *Thin Solid Films*, **292**, 135 (1997).
49. G. S. Higashi and C. G. Fleming, *Appl. Phys. Lett.*, **55**, 1963 (1989).
50. M. Ritala, H. Saloniemi, M. Leskela, T. Prohaska, G. Friedbacher, and M. Grasserbauer, *Thin Solid Films*, **286**, 54 (1996).
51. P. Ericsson, S. Bengtsson, and J. Skarp, *Microelectron. Eng.*, **36**, 91 (1997).
52. R. Matero, A. Rahtu, M. Ritala, M. Leskela, and T. Sajavaara, *Thin Solid Films*, **368**, 1 (2000).
53. H. Sato, T. Minami, S. Takata, T. Miyata, and M. Ishii, *Thin Solid Films*, **236**, 14 (1993).
54. B. Canava, J.-F. Guillemoles, E.-B. Yousfi, P. Cowache, H. Kerber, A. Loeffl, H.-W. Schock, M. Powalla, D. Hariskos, and D. Lincot, *Thin Solid Films*, **361-362**, 187 (2000).
55. T. K. Shioyama, U.S. Pat. 4,260,845 (1981).
56. R. L. Cobb, U.S. Pat. 4,568,784 (1986).
57. B. M. Welch, U.S. Pat. 4,692,430 (1987).
58. J. Wrzyszc, M. Zawadzki, J. Trawczynski, H. Grabowska, and W. Mista, *Appl. Catal. A*, **210**, 263 (2001).
59. J. Q. Xu, Q. Y. Pan, Y. A. Shun, and Z. Z. Tian, *Sens. Actuators B*, **66**, 277 (2000).
60. J. Q. Xu, Y. A. Shun, Q. Y. Pan, and J. H. Qin, *Sens. Actuators B*, **66**, 161 (2000).
61. J. W. Elam and S. M. George, *Chem. Mater.*, **15**, 1020 (2003).
62. J. W. Elam, M. D. Groner, and S. M. George, *Rev. Sci. Instrum.*, **73**, 2981 (2002).
63. M. D. Groner, J. W. Elam, F. H. Fabreguette, and S. M. George, *Thin Solid Films*, **413**, 186 (2002).
64. *CRC Handbook of Chemistry and Physics*, 63rd ed., R. C. Weast and M. J. Astle, Editors, CRC Press, Inc., Boca Raton, FL (1982-1983).
65. C. J. F. Bottcher, *Theory of Electric Polarization*, Elsevier Publishing, Amsterdam (1952).
66. M. Born and E. Wolf, *Principles of Optics*, Pergamon Press, Oxford (1975).
67. A. Paranjpe, S. Gopinath, T. Omstead, and R. Bubber, *J. Electrochem. Soc.*, **148**, G465 (2001).
68. H. Kim, A. Pique, J. S. Horwitz, H. Murata, Z. H. Kafafi, C. M. Gilmore, and D. B. Chrisey, *Thin Solid Films*, **377-378**, 798 (2000).
69. J. Hu and R. G. Gordon, *J. Appl. Phys.*, **71**, 880 (1992).
70. A. F. Aktaruzzaman, G. L. Sharma, and L. K. Malhotra, *Thin Solid Films*, **198**, 67 (1991).
71. H.-K. Kim, S.-H. Han, T.-Y. Seong, and W.-K. Choi, *J. Electrochem. Soc.*, **148**, G114 (2001).
72. J. M. Jensen, A. B. Oelkers, R. Toivola, D. C. Johnson, J. W. Elam, and S. M. George, *Chem. Mater.*, **14**, 2276 (2002).